

## Small-Angle X-ray Scattering Analysis of Particle-Size Distributions of Mesoscopic Metallic Systems with Consideration of the Particle Form Factor

BY H. G. KRAUTHÄUSER, W. HEITMANN, A. KOPS AND G. NIMTZ

II. Physikalisches Institut, Universität zu Köln, Zùlpicher Strasse 77, 50937 Köln, Germany

(Received 16 April 1993; accepted 11 January 1994)

### Abstract

The size distribution of mesoscopic metallic systems is determined by small-angle X-ray scattering using the indirect transformation method. It was found that a system of indium particles in an oil matrix can be best fitted if the particles are assumed to be homogeneous spheres. This assumption does not hold for a system of nickel in SiO<sub>2</sub>: to get a good approximation to the measured data, the form factor has to be refined. By comparison of the obtained particle-size distributions with theoretical models for different growth processes, it is possible to distinguish between Ostwald ripening and coalescence growth of the particles during the preparation.

### I. Introduction

Small-angle scattering of X-rays (SAXS) is an important method for determination of particle sizes in the range up to 100 nm integrating over a macroscopic sample volume. As the number of particles in the illuminated sample can easily exceed 10<sup>12</sup>, small-angle X-ray scattering is a very useful method for the determination of particle-size distributions.

With the assumption of a dilute and isotropic sample of randomly orientated particles having the same shape but different size (linear size parameter  $R$ ) in a homogeneous matrix, the particle-size distribution  $D_n(R)$  can be obtained from the smeared scattering intensities  $\tilde{I}(h)^*$  according to (Glatter & Kratky, 1982; Vonk, 1976)

$$\tilde{I}(h) = 2I_e \int_{x_1}^{x_2} \int_0^{t_2} \int_{\lambda_1}^{\lambda_2} \int_{R_1}^{R_2} Q(x)[P * \Pi_{DS}](t) \times W(\lambda') D_n(R) m^2(R) \phi(\beta) dR d\lambda' dt dx \quad (1)$$

with

$$\beta = R[(h - x)^2 + t^2]^{1/2} / \lambda'. \quad (2)$$

In this equation,  $h = (4\pi/\lambda_0) \sin \Theta$  is the absolute value of the scattering vector ( $\Theta$  is half of the

scattering angle and  $\lambda_0$  is the central wavelength of the primary radiation),  $I_e$  is the scattering intensity for a single electron,  $Q(x)$  is the beam-width profile,  $P(t)$  is the beam-length profile and  $W(\lambda')$  is the wavelength profile with  $\lambda' = \lambda/\lambda_0$ . The beam-length profile  $P(t)$  has to be convoluted with a step function  $\Pi_{DS}$  of the length of the detector slit. The factor  $m(R)$  includes the electron-density distribution of the scattering particle: it is the integral over the excess electron-density distribution over the volume of the particle. The last and very important factor in (1) is the particle form factor  $\phi(\beta)$  (here, the form factor is the scattering intensity of a single particle averaged over all orientations and normalized to unity in the forward-scattering direction).

The most important special case for the form factor is a system of homogeneous spheres with radius  $R$ . In this case, the form factor is given by

$$\phi_{\text{sphere}}(hR) = \{3[\sin(hR) - hR \cos(hR)]/(hR)^3\}^2. \quad (3)$$

The case of homogeneous spheres can be generalized to a system of randomly orientated homogeneous spheroids with axes ( $2R, 2R, \nu 2R$ ). The form factor for such a system follows from (3) with an additional integration (Guinier & Fournet, 1955):

$$\phi_{\text{spheroid}}(hR) = \int_0^{\pi/2} \phi_{\text{sphere}}(hR\xi) \cos \Theta d\Theta \quad (4)$$

with

$$\xi = (\cos^2 \Theta + \nu^2 \sin^2 \Theta)^{1/2}. \quad (5)$$

The factor  $\nu$  is the ratio of the two symmetry axes.

### II. Method

#### A. Instrumentation

The SAXS curves are measured using a Kratky small-angle camera with secondary monochromator and scintillation counter with the multiple scanning technique (Zipper, 1972). The radiation is supplied from a rotating-anode tube (copper target,  $\lambda_0 = 0.15405$  nm) with an acceleration voltage  $U = 40$  kV and a tube current  $I = 300$  mA.

\* The intensities  $\tilde{I}(h)$  are only corrected for dead time, dark current and blank scattering.

Since the tube focus is very small, the investigations of Stabinger & Kratky (1979) for the 'integrated camera' are applicable: by removal of the entrance slit of the Kratky camera, the intensity can be increased by a factor of three. The laboratory has to be held at constant temperature (here  $\pm 0.25$  K) to ensure the position of the camera relative to the tube focus remains constant (Heitmann, Krauthäuser, Kops & Nitz, 1994).

Usually, the Kratky camera is evacuated to avoid parasitic scattering. It has been proved by the authors that a helium atmosphere in the camera does not provoke more parasitic scattering than a vacuum. So it is now possible to examine samples that cannot be put into a vacuum without any foils between sample and camera volume (Heitmann *et al.*, 1994).

The wavelength profile  $W(\lambda')$  was measured very accurately using an Si (111) single crystal at a large-angle diffractometer mounted in front of the second beam window of the same tube.

### B. The indirect transformation method

The evaluation of the particle-size distribution from the scattering intensities was done by means of the indirect transformation method, developed by Glatter (1977, 1980).

The indirect transformation method starts with a linear expansion for the size distribution:

$$D_n(R) = \sum_{v=1}^N c_v \varphi_v(R). \quad (6)$$

Here,  $\varphi_v(R)$  are equidistant cubic  $B$ -spline functions (Greville, 1969; Schelten & Hossfeld, 1971). The expansion coefficients have to be determined. The number of spline functions,  $N$ , is limited by numerical considerations so that the size distribution is assumed to be band-limited. The spline functions can be transformed into the 'measuring space' according to (1). This transformation leads to an approximation  $I_A(h)$  for the measured intensities:

$$I_A(h) = \sum_{v=1}^N c_v \chi_v(h), \quad (7)$$

where the  $\chi_v(h)$  are the Fourier-transformed and smeared spline functions  $\varphi_v(R)$ . The unknown coefficients  $c_v$  are determined by solving a normal equation according to the extended least-squares condition

$$\begin{aligned} L + \lambda N_c &= \sum_{i=1}^M \left[ \tilde{I}(h_i) - \sum_{v=1}^N c_v \chi_v(h_i) \right]^2 / \sigma(h_i)^2 \\ &+ \lambda \sum_{v=1}^{N-1} (c_{v+1} - c_v)^2 \\ &= \min. \end{aligned} \quad (8)$$

In this equation,  $\lambda N_c$  is a damping term for the coefficient vector  $c_v$ . The damping is regulated by the Lagrange multiplier  $\lambda$ .

### C. Computation

The calculations are performed using Glatter's (1977) Fortran program system ITP-81 on an HP9000/720 workstation. The program code was optimized to give an increase of a factor of three in speed. Also, the routines for calculating the Fourier transformation for polydisperse systems with a given form factor (no spheres) were rewritten to guarantee a very accurate consideration of the form factor even for large values of  $hR$  [see (4)].

## III. Experimental results

### A. Indium in oil

Fig. 1 shows the smeared scattering intensities  $\tilde{I}(h)$  for a system of indium particles in an oil matrix together with two independent approximations. The indium system was produced using the VERL method (VERL = vacuum evaporation on a running liquid) (Nitz, Marquardt & Gleiter, 1988). The volume fraction of the indium particles is  $\Phi = 0.018$ . The oil is polyetherpolyol Baygal<sup>®</sup> K 390.

The two approximations to the measured data are a polydisperse system of homogeneous spheres and a polydisperse system of randomly orientated homogeneous spheroids with  $\nu = 1.1$ . The system of spheres leads to a more satisfactory approximation of the measured data than the system of spheroids.

The particle-size distribution  $D_n(R)$  according to the approximation of a system of homogeneous spheres is shown in Fig. 2. The other two curves shown in this figure are theoretical size distributions, which will be discussed later.

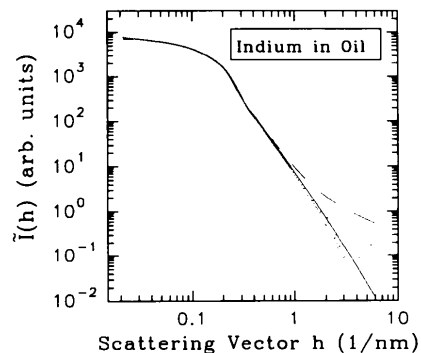


Fig. 1. Smeared scattering intensities  $\tilde{I}(h)$  versus the absolute value of the scattering vector  $h$ . Points give experimental intensities for a system of indium in oil (volume fraction  $\Phi = 0.018$ ); — best approximation of a system of homogeneous spheres; - - - best approximation of a system of homogeneous spheroids with  $\nu = 1.1$

### B. Nickel in SiO<sub>2</sub>

The scattering intensities  $\tilde{I}(h)$  of a system of nickel in SiO<sub>2</sub> are shown in Fig. 3. The system was produced by a sol-gel process. The volume fraction of the nickel particles is about  $\Phi = 0.2$ . In this figure, the best approximations according to a system of homogeneous spheres and a system of homogeneous spheroids with  $\nu = 1.2$  are also represented. The approximation according to a system of spheroids is nearly perfect over the whole measuring range compared with a system of spheres.

Fig. 4 shows the particle-size distribution according to the approximation for the spheroid system from Fig. 3. The solid line is a theoretical size distribution, which will be discussed later.

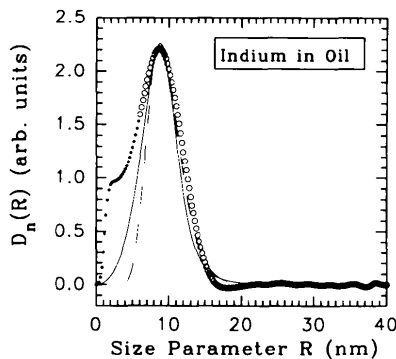


Fig. 2. Particle-size distributions  $D_n(R)$  versus the particle size  $R$ .  $\circ$  Distribution according to the system of homogeneous spheres (see Fig. 1). The range strongly influenced by errors owing to the evaluation method is marked by smaller circles. — log-normal distribution with  $R_0 = 9$  nm and  $\sigma = 1.28$ ; — time-independent Ostwald distribution for  $\bar{R} = 9$  nm and volume fraction  $\Phi = 0.018$ .

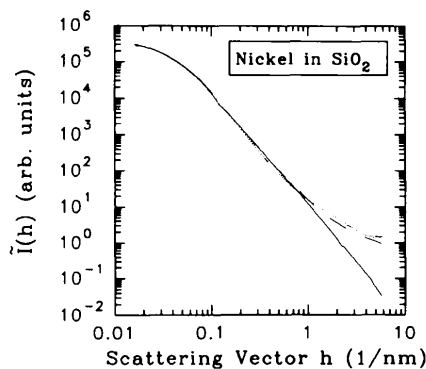


Fig. 3. Smearred scattering intensities  $\tilde{I}(h)$  versus the absolute value of the scattering vector  $h$ . Points show experimental intensities for a system of nickel in SiO<sub>2</sub> (volume fraction  $\Phi = 0.2$ ); — best approximation of a system of homogeneous spheres; — — best approximation of a system of homogeneous spheroids with  $\nu = 1.2$ .

### C. Electron-microscopy data

One of the systems discussed here – indium in Baygal – has been analyzed using transmission electron microscopy (TEM). From these investigations, it follows that: most of the particles are isolated but there are also large clusters of agglomerated particles; the isolated particles can be assumed to be spherical; the mean radius of the particles is 7.5 nm.

Since the samples have to be diluted for the TEM investigations, it is very probably that the agglomeration of the particles is an artifact of TEM preparation.

## IV. Discussion

### A. Particle growth

1. *Coalescence growth.* A statistical analysis of the coalescence growth of particles leads to the result that the logarithm of the particle volume is Gaussian (Granqvist & Buhrman, 1976). So it follows that the distribution of the particle-size parameter  $R$  is a log-normal distribution. The (normalized) log-normal distribution is given by

$$f_{LN}(R) = 1/[(2\pi)^{1/2}(\ln \sigma)] \times \exp[-(\ln R - \ln R_0)^2/2 \ln^2 \sigma]. \quad (9)$$

Here,  $\sigma$  is the standard deviation (dimensionless and larger than unity) and  $R_0$  is the most probable particle size. Following Granqvist & Buhrman (1976), typical values for the standard deviations are in the range

$$1.1 \leq \sigma \leq 1.6. \quad (10)$$

2. *Ostwald ripening.* The first theoretical considerations of Ostwald ripening were given by Lifshitz & Slyozov (1961) and Wagner (1961). This theory – well known as the LSW theory of Ostwald ripening – is only valid in the limits of infinite dilution of the system. Modifications to the LSW theory for the case

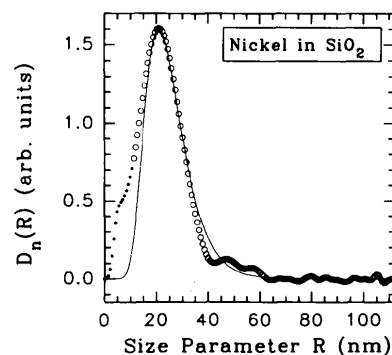


Fig. 4. Particle-size distribution  $D_n(R)$  versus the particle size  $R$ .  $\circ$  Distribution according to the system of homogeneous spheroids (see Fig. 3). The range strongly influenced by errors owing to the evaluation method is marked by smaller circles; — log-normal distribution with  $R_0 = 21$  nm and  $\sigma = 1.4$ .

of finite volume fractions,  $\Phi \neq 0$ , are given by Ardell (1972) and later by Voorhees & Glicksman (1984; Voorhees, 1985). The particle-size distribution for Ostwald ripening,  $f(\tau, \rho, \Phi)$ , can be expressed as a product of two functions:

$$f(\tau, \rho, \Phi) = g(\tau)h(\rho, \Phi), \quad (11)$$

where  $\tau$  is a dimensionless time and  $\rho$  is a dimensionless size parameter, defined as the particle size  $R$  normalized to the mean particle size  $\bar{R}$ . Following the considerations of Voorhees & Glicksman, the time-independent size distribution  $h(\rho, \Phi)$  can be calculated numerically. The resulting distributions are shown in Fig. 5 for several values of the volume fraction  $\Phi$ .

### B. Indium in oil

It was shown that the scattering intensities for the system of indium in oil can be best fitted assuming the particles are homogeneous spheres. This is a very astonishing result because – owing to strong symmetry – the form factor of spheres shows a very typical and restrictive behavior. The transition from a system of spheres to a system of spheroids can be regarded as a step from an ideal (theoretical) system to a real system: any deviation from the ideal ‘system of homogeneous spheres’ breaks up the strong symmetry and smooths out the form factor in a typical way.

So, in most cases, the form factor of real systems looks more like the form factor of a system of spheroids than that of a system of spheres. This emphasizes that the indium particles in the oil matrix are indeed spherical.

The particle-size and -shape information following from SAXS measurements is in agreement with that obtained from TEM investigations but it is more detailed.

To interpret the obtained particle-size distribution, shown in Fig. 2, the data are compared with particle-size distributions obtained from theoretical considerations.

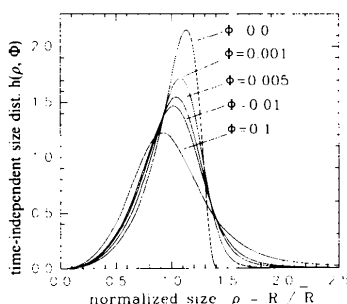


Fig. 5. Normalized time-independent size distributions  $h(\rho, \Phi)$  versus the normalized size  $\rho$  for different values of the volume fraction  $\Phi$ .

The first model is coalescence growth of the particles. As shown before, a statistical growth analysis of coalescence growth leads to a log-normal distribution of the particle size (here the radius). Secondly, the extended model of Ostwald ripening was chosen. Two curves according to these theoretical models are shown in Fig. 2 together with the particle-size distribution obtained from the best approximation to the scattering intensities. Both models lead to a good approximation in the middle and the outer part of the curve ( $R > 6$  nm). In the central part ( $R < 6$  nm), Ostwald ripening gives a better result but does not fit the experimental data satisfactorily. It must be emphasized that the time-independent Ostwald distribution is fully determined by the well known volume fraction of the system, the mean size and the peak value of the distribution. In fact, there is no free parameter for the Ostwald distribution.

In contrast to the Ostwald distribution, the slope of the log-normal distribution (owing to coalescence growth) is adjustable in a wide range by changing the standard deviation  $\sigma$ .

Hence, there is a greater possibility for the log-normal distribution to fit any given size distribution more satisfactorily than for the Ostwald distribution.

The central part of the particle-size distribution ( $R < 6$  nm) is hardly influenced by the choice of the Lagrange multiplier  $\lambda$ . So the interpretation of this part of the curve is obscure.

### C. Nickel in SiO<sub>2</sub>

In contrast to the system discussed above, in the case of nickel in SiO<sub>2</sub> it was shown that a variation of the form factor could improve the approximation to the measured data. From this, more information on the sample can be obtained.

The alternatives for interpreting the results are: (1) the system of nickel in SiO<sub>2</sub> is really a system of homogeneous spheroids with axes  $(2R, 2R, \nu 2R)$ ; (2) the system is neither a system of homogeneous spheres nor a system of homogeneous spheroids but a system of which the form factor looks more like that of a system of spheroids than that of a system of spheres. The second case would be true if all the particles cannot be assumed to have exactly the same shape. If one takes the preparation process into account, the second possibility is more probable.

A comparison was attempted between the particle-size distribution for the system of nickel in SiO<sub>2</sub>, shown in Fig. 4, and particle-size distributions according to coalescence growth and Ostwald ripening. Owing to the large volume fraction, the Ostwald distribution according to this system is very broad and does not fit the experimental data – it is not presented in Fig. 4. As one can see in this figure, the

log-normal distribution leads to a good approximation of the obtained particle-size distribution (the misfit in the central part ( $R < 10$  nm) of the curve is not interpreted because of the artifact discussed above for the system of indium in oil).

Hence, by analysis of the particle-size distribution, it was shown that the model of Ostwald ripening can be rejected for this system.

### V. Concluding remarks

The SAXS investigations have shown that

(a) particle-size distributions can be evaluated from scattering data;

(b) if the quality of approximation for different particle form factors is monitored, it is possible to distinguish between spherical and non-spherical systems;

(c) the obtained particle-size distributions are in agreement with theoretical models of particle growth;

(d) for the system indium in oil (volume fraction  $\Phi = 0.018$ ), one cannot distinguish between Ostwald ripening and coalescence growth because the theoretical distributions are very similar. Of course, it is less probable for the Ostwald distribution to fit the data purely by chance;

(e) for the system nickel in  $\text{SiO}_2$  (volume fraction  $\Phi = 0.2$ ), the particle-size distribution is in good agreement with a log-normal distribution. So for this system it is possible to distinguish between Ostwald ripening and coalescence growth.

The authors gratefully acknowledge H. Eifert (Fraunhofer-Institut für angewandte Materialfor-

schung, Bremen) for the preparation of the indium systems and Dr K. Rose (Fraunhofer-Institut für Silicatforschung, Würzburg) for the preparation of the nickel system. The research was sponsored by the Bundesministerium für Forschung und Technologie (project 03M 2737B2) and the Deutsche Forschungsgemeinschaft (SFB 341 A3).

### References

- ARDELL A. J. (1972). *Acta Metall.* **20**, 61–71.  
 GLATTER, O. (1977). *J. Appl. Cryst.* **10**, 415–421.  
 GLATTER, O. (1980). *J. Appl. Cryst.* **13**, 7–11.  
 GLATTER, O. & KRATKY, O. (1982). *Small-Angle X-ray Scattering*. New York: Academic Press.  
 GRANQVIST, C. G. & BUHRMAN, R. A. (1976). *J. Appl. Phys.* **47**, 2200–2219.  
 GREVILLE, T. N. E. (1969). *Theory and Applications of Spline Functions*. New York: Academic Press.  
 GUINIER, A. & FOURNET, G. (1955). *Small-Angle Scattering of X-rays*. New York: Wiley.  
 HEITMANN, W., KRAUTHÄUSER, H. G., KOPS, A. & NIMTZ, G. (1994). *J. Appl. Cryst.* Submitted.  
 LIFSHITZ, I. M. & SLYOZOV, V. V. (1961). *J. Phys. Chem. Solids*, **19**, 35–50.  
 NIMTZ, G., MARQUARDT, P. & GLEITER, H. (1988). *J. Cryst. Growth*, **86**, 66–71.  
 SCHELLEN, J. & HOSSFELD, F. (1971). *J. Appl. Cryst.* **4**, 210–223.  
 STABINGER, H. & KRATKY, O. (1979). *Makromol. Chem.* **180**, 2995–2997.  
 VONK, C. G. (1976). *J. Appl. Cryst.* **9**, 433–440.  
 VOORHEES, P. W. (1985). *J. Statist. Phys.* **38**, 231–252.  
 VOORHEES, P. W. & GLICKSMAN, M. E. (1984). *Acta Metall.* **32**, 2001–2011, 2013–2030.  
 WAGNER, G. (1961). *Z. Elektrochem.* **65**, 581–591.  
 ZIPPER, P. (1972). *Acta Phys. Austriaca*, **36**, 27–38.